Chemical Science

ROYAL SOCIETY OF CHEMISTRY

EDGE ARTICLE

View Article Online
View Journal | View Issue

Cite this: *Chem. Sci.*, 2021, **12**, 13469

All publication charges for this article have been paid for by the Royal Society of Chemistry

Received 9th July 2021
Accepted 12th September 2021

DOI: 10.1039/d1sc03751j

rsc.li/chemical-science

Self-assembly of a water-soluble endohedrally functionalized coordination cage including polar guests†

Qingqing Sun, ‡[ab] Luis Escobar, §*[ab] Jorn de Jong ¶[a] and Pablo Ballester *[ac]

Coordination cages containing endohedrally functionalized aromatic cavities are scarce in the literature. Herein, we report the self-assembly of a tetra-cationic super aryl-extended calix[4]pyrrole tetra-pyridyl ligand into a water-soluble Pd(II)-cage featuring two endohedral polar binding sites. They are defined by the four pyrrole NHs of the calix[4]pyrrole unit and the four inwardly directed α-protons of the coordinated pyridyl groups. The efficient assembly of the Pd(II)-cage requires the inclusion of mono- and ditopic pyridyl *N*-oxide and aliphatic formamide guests. The monotopic guests only partially fill the cage's cavity and require the co-inclusion of a water molecule that is likely hydrogen-bonded to the endohedral α-pyridyl protons. The ditopic guests are able to completely fill the cage's cavity and complement both binding sites. We observed high conformational selectivity in the inclusion of the isomers of α,ω-bis-formamides. We briefly investigate the uptake and release mechanism/kinetics of selected polar guests by the Pd(II)-cage using pair-wise competition experiments.

Introduction

Self-assembly is an effective synthetic strategy for the construction of coordination cages (CCs) in organic solvents and in water.[1–3] Their molecular components are multitopic aromatic ligands (L) and metal coordination ions (M).[4] The inclusion of size, shape and charge complementary guests in CCs enables not only selective molecular recognition but also controls the properties, reactivities and the confinement and release of molecular cargo.[3,5–8] The inclusion of polar guests requires the functionalization of the CCs' cavities with polar groups.[9,10] However, the extensive use of aromatic panels in shaping the cavity makes this endeavour synthetically difficult. Fujita and co-workers introduced a strategy to generate spherical $[L_{24}\cdot Pd_{12}]^{24+}$ CCs containing 24 inwardly directed functional groups.[11] Subsequently, Reek and co-workers applied the strategy to develop catalyst systems.[12] In addition, $[L_4\cdot Pd_2]^{4+}$ CCs (Fig. 1a) were assembled from bis-pyridyl ligands featuring imide,[13] amide[14] or urea[15,16] groups as spacing units. The 4 ligands were located at the edges of the CCs' cavity and the NH hydrogen bond donors were placed in a way that they were inwardly directed. The $[L_4\cdot Pd_2]^{4+}$ CCs bearing endohedral amide or urea NHs bound glycosides in organic solvents owing to the establishment of intermolecular hydrogen-bonding and CH–π interactions.[14,16] In the same vein, tetrahedral $[L_6\cdot M_4]^{8+}$ CCs (Fig. 1b) featuring inwardly directed urea NHs,[17–19] hydroxyl[20] or carboxylic acid[21,22] groups have been reported in the literature. Martinez, Nitschke and co-workers reported the anion-templated self-assembly of an azaphosphatrane endohedrally functionalized $[L_4\cdot Fe_4]^{12+}$ CC (Fig. 1c) in aqueous solution.[23] The $[L_4\cdot Fe_4]^{12+}$ CC was capable of selective anion extraction and recovery.[24]

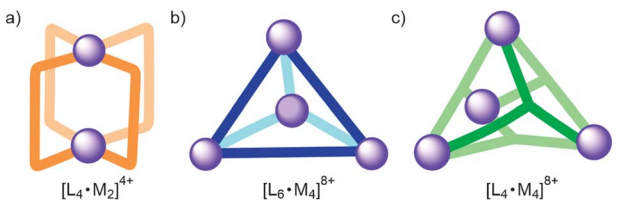

Fig. 1 Schematic representation of different CCs previously reported in the literature: (a) $[L_4\cdot M_2]^{4+}$, (b) $[L_6\cdot M_4]^{8+}$ and (c) $[L_4\cdot M_4]^{8+}$. Ligands (L) contain inwardly directed functional groups, which are not shown for clarity.

[a]*Institute of Chemical Research of Catalonia (ICIQ), The Barcelona Institute of Science and Technology (BIST), Av. Països Catalans 16, 43007 Tarragona, Spain. E-mail: pballester@iciq.es*

[b]*Universitat Rovira i Virgili (URV), Departament de Química Analítica i Química Orgánica, c/Marcel·lí Domingo 1, 43007 Tarragona, Spain*

[c]*ICREA, Passeig Lluís Companys 23, 08010 Barcelona, Spain*

† Electronic supplementary information (ESI) available: CCDC 2093909–2093911. For ESI and crystallographic data in CIF or other electronic format see DOI: 10.1039/d1sc03751j

‡ Present address: Yangzhou University, School of Chemistry and Chemical Engineering, Yangzhou, 225002 Jiangsu, China.

§ Present address: Ludwig-Maximilians-Universität München (LMU), Department of Chemistry, Butenandtstrasse 5-13, 81377 München, Germany. E-mail: luis.escobar@cup.lmu.de

¶ Present address: Leiden University, Leiden Institute of Chemistry, Einsteinweg 55, 2333 CC Leiden, The Netherlands.

Recently, we described the self-assembly of the $[\mathbf{1a}\cdot Pd]^{2+}$ CC in a 2 : 1 $CDCl_3/CD_3CN$ solution mixture[25] (Fig. 2a and 3b). The tetra-pyridyl chelating ligand **1a** is based on a "four-wall" super aryl-extended calix[4]pyrrole (SAE-C[4]P) scaffold. The $[\mathbf{1a}\cdot Pd]^{2+}$ CC might also be considered as a mono-nuclear metal-coordinated cavitand. The use of coordination metals in controlling the conformations and binding properties of covalent organic hosts has also been reported by the groups of de Mendoza,[60,61] Badjić[26–28] and Rebek.[29–33] The $[\mathbf{1a}\cdot Pd]^{2+}$ CC features two different and converging polar binding sites[34] defined by the four pyrrole NHs of the C[4]P unit and the four inwardly directed α-CH protons of the pyridyl groups coordinated to Pd(II). The assembly of the CC requires the filling of its cavity with suitable polar guests. The bound guests not only fill *ca.* 55% of the cavity volume[35] but also satisfy the hydrogen-bonding characteristics of the two polar binding sites (Fig. 3b). We also investigated the inclusion/exchange mechanisms of the guests operating in the $[\mathbf{1a}\cdot Pd]^{2+}$ CC.[36] We proposed a "French doors" mechanism[37] for the in/out exchange of planar pyridyl *N*-oxide derivatives. For more sterically demanding guests, we postulated an alternative process involving a partial ligand–metal dissociation mechanism.

Herein, we report the self-assembly of a structurally related CC, $[\mathbf{2}\cdot Pd]^{6+}$, in water solution. We describe the synthesis of the tetra-cationic ligand precursor $\mathbf{2}^{4+}$ (Fig. 2a). The formation of the $[\mathbf{2}\cdot Pd]^{6+}$ CC follows the assembly principles described above for the $[\mathbf{1a}\cdot Pd]^{2+}$ counterpart. We show that the CC's assembly only occurs upon including mono- and ditopic pyridyl *N*-oxides, as well as aliphatic mono- and bis-formamide guests. All the polar guests used are difficult to bind in water solution with other synthetic receptors.[38–40] Using ^{1}H NMR spectroscopy, we study the conformational arrangement adopted by the end formyl groups of the α,ω-bis-formamides included in the $[\mathbf{2}\cdot Pd]^{6+}$ CC. We disclose solid-state structures for analogous inclusion complexes with the organic-soluble $[\mathbf{1a}\cdot Pd]^{2+}$ CC. Finally, we investigate the uptake and release mechanisms of selected polar guests in the $[\mathbf{2}\cdot Pd]^{6+}$ CC using competitive, pair-wise binding experiments.

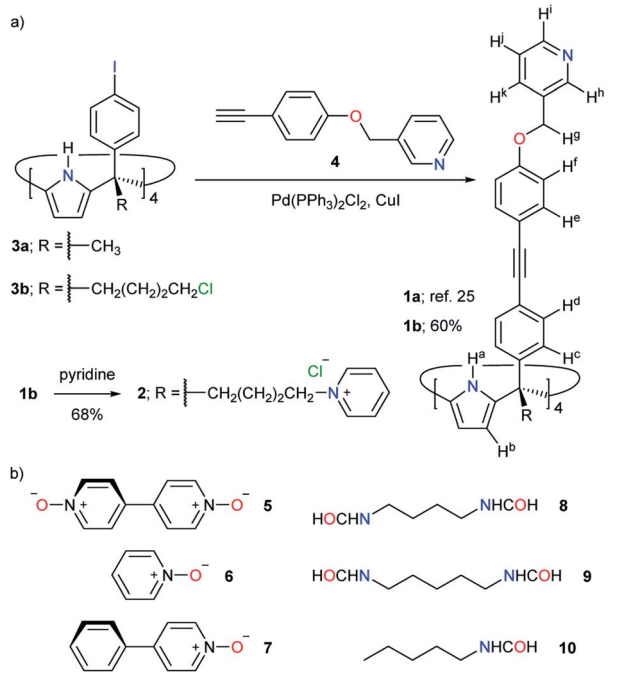

Fig. 2 (a) Synthesis of tetra-pyridyl SAE-ligands **1a**, **1b** and **2**. (b) Line-drawing structures of guests **5**–**10** used in this study.

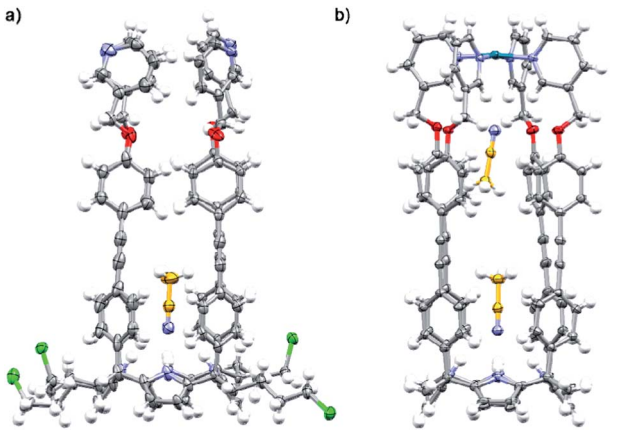

Fig. 3 X-ray crystal structures of (a) **1b** and (b) $[\mathbf{1a}\cdot Pd]^{2+}$. The structures are shown in ORTEP view with thermal ellipsoids set at 50% probability for the non-hydrogen atoms. Hydrogen atoms are depicted as fixed-size spheres of 0.3 Å radius.

Results and discussion

Synthesis of tetra-pyridyl SAE-C[4]P ligands 1b and $\mathbf{2}^{4+}$

The tetra-cationic SAE-ligand $\mathbf{2}^{4+}$ was synthesized in two steps starting from the tetra-α isomer of 4-iodophenyl-4′-chlorobutyl C[4]P **3b**[41] (Fig. 2a). Firstly, the quadruple Sonogashira cross-coupling reaction between tetra-iodo C[4]P **3b** and pyridyl mono-acetylene **4**[25] afforded, after column chromatography purification, the tetra-chloro SAE-ligand **1b** in 60% yield. Next, we treated **1b** with excess of pyridine at 110 °C affording the tetra-chloride salt of $\mathbf{2}^{4+}$ in 68% yield. Both SAE-ligands, **1b** and $\mathbf{2}^{4+}$, were fully characterized using a set of high-resolution spectra (ESI†).

The tetra-chloro SAE-ligand **1b** was also characterized by X-ray diffraction of a single crystal grown from a 1 : 1 CH_2Cl_2/CH_3CN solution mixture (Fig. 3a). In the solid state, **1b** adopts the cone conformation by including one molecule of CH_3CN. The nitrogen atom of the included CH_3CN is hydrogen-bonded to the four pyrrole NHs of the C[4]P unit ($d_{average}$ (N···N) ∼ 3.3 Å). Moreover, the aromatic cavity of the upper section of **1b** collapses owing to the establishment of intramolecular π–π interactions.[42]

The neutral tetra-pyridyl SAE-ligand **1b** self-assembled almost quantitatively into the $[\mathbf{1b}\cdot Pd]^{2+}$ CC in a 2 : 1 $CDCl_3/CD_3CN$ solution mixture by addition of *ca.* 1 equiv. of $[Pd(CH_3CN)_4(BF_4)_2]$ (Fig. S14†). Consequently, the *meso*-alkyl substituents of **1b** did not have an impact on the assembly of the CC.

Attempts to self-assemble the $[2\cdot Pd]^{6+}$ CC in the absence of guests

We probed the analogous coordination of Pd(II) with the water-soluble tetra-pyridyl SAE-ligand 2^{4+} (Fig. 2a) by means of ^{1}H NMR spectroscopy. At 298 or 333 K, the ^{1}H NMR spectrum of 2^{4+} in the D_2O solution showed very broad proton signals‖ (Fig. S31† and 4a, respectively). However, the addition of *ca.* 10% DMSO to the D_2O solution of 2^{4+} at r.t. provoked the appearance of sharp proton signals (Fig. S82†). Taken together, these observations indicated that the SAE-ligand 2^{4+} experienced significant aggregation in water solution. We cannot rule out the possibility that the aggregation process also makes the conformational exchange dynamics (cone and alternate) of 2^{4+} become intermediate on the chemical shift time scale.

The putative assembly of $[2\cdot Pd]^{6+}$ would assign an overall six positive charges to the CC. For this reason, we expected that the increase in the repulsive coulombic interactions will induce a reduction in the aggregation tendency of $[2\cdot Pd]^{6+}$ compared to that of the parent SAE-ligand 2^{4+}. Nevertheless, the addition of *ca.* 1 equiv. of $Pd(NO_3)_2$ to the D_2O solution of 2^{4+} at r.t. produced a suspension. We surmised that the insoluble material originated from the formation of metal-mediated polymeric aggregates. The analysis of the filtered solution, at 333 K, showed broad proton signals, which did not support the presence of the CC in water.

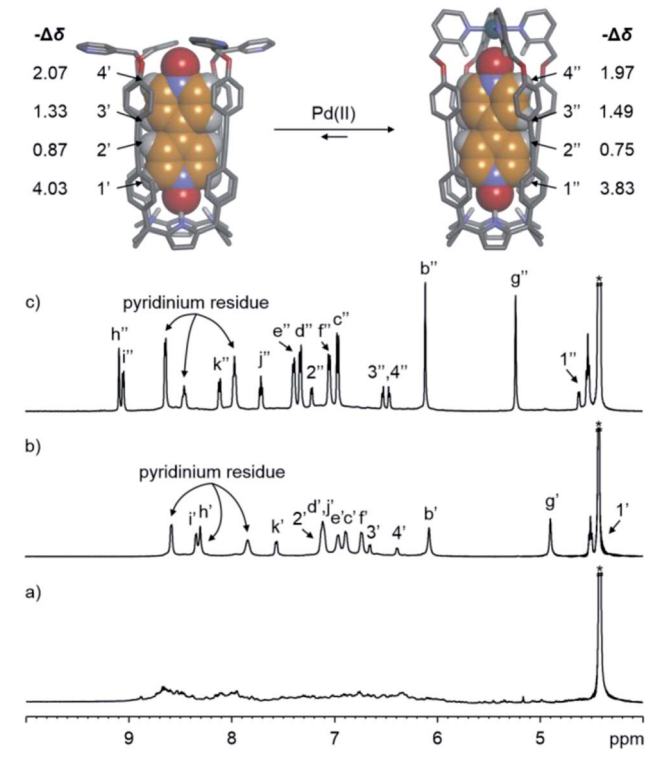

Fig. 4 (Top) Energy minimized structures (MM3) of the simplified $5\subset 2^{4+}$ and $5\subset[2\cdot Pd]^{6+}$ inclusion complexes. (Bottom) Selected regions of the ^{1}H NMR (500 MHz with a cryoprobe, D_2O, 333 K) spectra of (a) 2^{4+}, (b) $5\subset 2^{4+}$ and (c) $5\subset[2\cdot Pd]^{6+}$. Primed and double primed labels correspond to the proton signals of $5\subset 2^{4+}$ and $5\subset[2\cdot Pd]^{6+}$, respectively. See Fig. 2a for the proton assignment of bound 2^{4+}. *Residual solvent peak.

Self-assembly of the $[2\cdot Pd]^{6+}$ CC in the presence of pyridine *N*-oxide guests

As stated above, the emergence of the $[\mathbf{1a}\cdot Pd]^{2+}$ CC (Fig. 3b) in organic solvents required the inclusion of suitable polar guests. One molecule of 4,4′-bis-pyridine *N*,*N*′-dioxide **5** or a combination of one pyridine *N*-oxide **6** (Fig. 2b) and one CH_3CN were perfect fits.[25,36] The *N*-oxides formed 1 : 1 inclusion complexes with the SAE-ligand **1a**. The bound ligand was locked in the cone conformation and its pyridyl residues were pre-organized for tetra-coordination to Pd(II).

At 333 K, the ^{1}H NMR spectrum of a D_2O solution containing equimolar amounts of the SAE-ligand 2^{4+} and the bis-*N*-oxide **5** displayed a set of well-defined proton signals in agreement with the C_{4v} symmetry of the receptor (Fig. 4b). Specifically, the two α-pyridyl protons of 2^{4+}, H^h and H^i, resonated at 8.30 and 8.34 ppm, respectively. The four aromatic protons of the *meso*-biphenyl-ethynyl substituents, H^c–H^f, emerged as separate signals (Fig. 4b). The β-pyrrole protons, H^b, appeared as a singlet at 6.07 ppm. The symmetry loss and the upfield shifts experienced by the protons of **5** placed it in the polar and deep aromatic cavity of 2^{4+} (Fig. 4, top panel).

The addition of more than 1 equiv. of **5** did not produce changes in the proton signals of 2^{4+}, but caused the emergence of those of the free guest (ESI†). All these observations supported the formation of the $5\subset 2^{4+}$ inclusion complex, which featured slow exchange dynamics on both the ^{1}H NMR and the EXSY time scales (t_{mix} = 0.3 s, Fig. S36†). We estimated a binding constant larger than 10^4 M^{-1}.

The complexation-induced shifts experienced by the aromatic protons of the bound bis-*N*-oxide **5** are not directly related to its depth in the aromatic cavity of 2^{4+} (see $-\Delta\delta$ values in Fig. 4, top panel). This result reflected the dissimilar magnetic anisotropy provided by the *meso*-biphenyl-ethynyl substituents of 2^{4+}.

The inclusion geometry of the $5\subset 2^{4+}$ complex diminishes the aromatic surface of the receptor available for water solvation. Because the binding of non-polar residues in water is mainly driven by the hydrophobic effect (HE),[38,43] the reduction in the aromatic surface helps explain the lower aggregation tendency of the $5\subset 2^{4+}$ complex compared to that of the free receptor 2^{4+}.

The addition of *ca.* 1 equiv. of $Pd(NO_3)_2$ to the D_2O solution of $5\subset 2^{4+}$ produced the complete disappearance of its proton signals and the emergence of a new set that was also in agreement with the C_{4v} symmetry of the SAE-ligand 2^{4+}. Based on our previous findings in organic solution,[25,36] the new set of signals was diagnostic of the $5\subset[2\cdot Pd]^{6+}$ CC complex (*vide infra*) (Fig. 4c). Using an internal standard, we calculated that the CC complex was assembled to a 60% extent. Most likely, metal-mediated aggregates of $5\subset 2^{4+}$ were also formed whose proton signals broadened beyond detection.

The formation of *N*-Pd(II) coordination bonds in the $5\subset[2\cdot Pd]^{6+}$ CC complex was substantiated by the downfield shifts

experienced by the two α-pyridyl protons, H^h and H^i ($\Delta\delta = +0.79$ and +0.71 ppm, respectively), with respect to their chemical shift values in the initial $\mathbf{5}\subset\mathbf{2}^{4+}$ complex. The reduced downfield shift experienced by the β-pyrrole protons, H^b, of $\mathbf{5}\subset[\mathbf{2}\cdot Pd]^{6+}$ indicated that the C[4]P unit maintained the cone conformation. Finally, the proton signals of **5** included in the CC suffered negligible chemical shift changes compared to those of $\mathbf{5}\subset\mathbf{2}^{4+}$. We reported analogous observations for the structurally related $\mathbf{5}\subset[\mathbf{1a}\cdot Pd]^{2+}$ CC assembled in organic solvents.[25]

The addition of **5** in excess did not produce chemical shift changes to the proton signals of the water-soluble $\mathbf{5}\subset[\mathbf{2}\cdot Pd]^{6+}$ CC complex (ESI†). The free and bound guest **5** was involved in a slow exchange process on both the ^{1}H NMR and the EXSY time scales (t_{mix} = 0.3 s, Fig. S39†). The binding constant of $\mathbf{5}\subset[\mathbf{2}\cdot Pd]^{6+}$ must be larger than 10^4 M^{-1}.

We performed a ^{1}H DOSY NMR experiment[44,45] using the D_2O solution containing the $\mathbf{5}\subset[\mathbf{2}\cdot Pd]^{6+}$ CC complex (Fig. S41†). The fit of the decay of all proton signals returned the diffusion constant value (D) of $\mathbf{5}\subset[\mathbf{2}\cdot Pd]^{6+}$ as $\log D = -9.31$. Collectively, the results presented above demonstrated that the emergence of the $[\mathbf{2}\cdot Pd]^{6+}$ CC in D_2O required the filling of its polar cavity with the bis-*N*-oxide **5**.** The assembly of the $[\mathbf{2}\cdot Pd]^{6+}$ CC was also studied at 333 K owing to the remaining aggregation problems at lower temperatures.††

In a 2 : 1 $CDCl_3/CD_3CN$ solution mixture, pyridine *N*-oxide **6** (Fig. 2b) was shown to be a good guest to induce the formation of the $\mathbf{6}\subset[\mathbf{1a}\cdot Pd]^{2+}$ CC complex.[25,36] X-ray crystallography revealed the co-inclusion of one CH_3CN molecule in the assembled $[\mathbf{6}\cdot CH_3CN]\subset[\mathbf{1a}\cdot Pd]^{2+}$ CC complex. We wondered if a water molecule could replace the CH_3CN for the co-inclusion of **6** in the water-soluble version of the CC.

At 333 K, the ^{1}H NMR spectrum of an equimolar D_2O solution (1 mM) of pyridine *N*-oxide **6** and the SAE-ligand $\mathbf{2}^{4+}$ showed a diminution in the broadening of the proton signals of the receptor/ligand (Fig. S43†). The protons of free **6** were visible as sharp signals with reduced intensity compared to those of a 1 mM solution. This result suggested that the $\mathbf{6}\subset\mathbf{2}^{4+}$ inclusion complex was formed to some extent. The subsequent addition of *ca.* 1 equiv. of $Pd(NO_3)_2$ provoked the appearance of a new set of sharp signals that were diagnostic of the assembly of the $\mathbf{6}\subset[\mathbf{2}\cdot Pd]^{6+}$ CC complex (Fig. S44†). We assumed that the co-inclusion of one molecule of water[46] with **6** took place. The putative $[\mathbf{6}\cdot H_2O]\subset[\mathbf{2}\cdot Pd]^{6+}$ CC complex (Fig. S88†) was assembled only to a 30% extent.

In agreement with the double role played by the bound guests in the CC complexes of $[\mathbf{1a}\cdot Pd]^{2+}$, 4-phenylpyridine *N*-oxide **7** (Fig. 2b) did not induce the emergence of the CC complex in 2 : 1 $CDCl_3/CD_3CN$.[25] Nevertheless, **7** formed a highly stable 1 : 1 inclusion complex with the SAE-ligand **1a** in the same solvent mixture. The addition of Pd(II) to the $\mathbf{7}\subset\mathbf{1a}$ complex resulted in the immediate appearance of metal-mediated oligomers. Owing to the reduced size of H_2O compared to CH_3CN, we were curious to find out if the co-inclusion of H_2O with **7** could induce the emergence of the $[\mathbf{7}\cdot H_2O]\subset[\mathbf{2}\cdot Pd]^{6+}$ CC complex.

The ^{1}H NMR spectrum of an equimolar mixture of **7** and $\mathbf{2}^{4+}$ in D_2O solution at 333 K showed the formation of the corresponding $\mathbf{7}\subset\mathbf{2}^{4+}$ inclusion complex. However, the extent to which the 1 : 1 complex was formed was lower than that in the case of the bis-*N*-oxide **5** (Fig. S47†). The subsequent addition of 1 equiv. of $Pd(NO_3)_2$ provoked the formation of metal-mediated aggregates of $\mathbf{2}^{4+}$, which may partially bind the *N*-oxide **7**. In short, the system expresses an analogous behaviour to the one observed in the mixture of organic solvents.[25]

Self-assembly of the $[\mathbf{2}\cdot Pd]^{6+}$ CC in the presence of aliphatic formamide guests

The successful results obtained with bis-*N*-oxide **5** prompted us to investigate the self-assembly of other inclusion complexes of the $[\mathbf{2}\cdot Pd]^{6+}$ CC in water solution using ditopic guests. Based on molecular modelling studies (MM3), we selected the aliphatic α,ω-bis-formamides **8** and **9**, having four and five methylene groups as spacers,[47] respectively (Fig. 2b). The extended conformations of both guests are good fits to the CC's cavity. In addition, the two end formyl groups of the bis-formamides can complement the two polar binding sites of the $[\mathbf{2}\cdot Pd]^{6+}$ CC.

At 333 K, the ^{1}H NMR spectrum of a 1 : 1 D_2O solution mixture of the bis-formamide **8** and the SAE-ligand $\mathbf{2}^{4+}$ did not display a set of sharp signals for the receptor (Fig. S51†). Yet, the signals of free **8** were easily detected. This result indicated that the putative $\mathbf{8}\subset\mathbf{2}^{4+}$ inclusion complex was formed to a reduced extent. Surprisingly, the addition of *ca.* 1 equiv. of $Pd(NO_3)_2$ to the above solution produced a set of sharp and well-defined signals corresponding to the $[\mathbf{2}\cdot Pd]^{6+}$ CC (Fig. 5a). We also observed two sets of signals for the protons of **8** with different intensities. The low intensity signals corresponded to the protons of the free guest. The more intense set displayed upfield shifts for all protons.

e assigned the latter to the protons of **8** included in the $[\mathbf{2}\cdot Pd]^{6+}$ CC. In short, the emergence of the $\mathbf{8}\subset[\mathbf{2}\cdot Pd]^{6+}$ CC complex was induced by the inclusion of **8** to an extent of 60% with respect to its molecular components.

One of the formyl protons of bound **8** displayed a significant upfield shift (*cis*″$_{lr}$, $\Delta\delta = -3.52$ ppm), placing it within the four *meso*-aryl substituents of the C[4]P unit[47,48] of the $[\mathbf{2}\cdot Pd]^{6+}$ CC (Fig. 5a, right). The other formyl proton also experienced a reduced magnetic shielding (*cis*″$_{ur}$, $\Delta\delta = -1.11$ ppm), owing to its inclusion in the upper aromatic cavity of the CC. The intermolecular cross-peaks present in a 2D ROESY experiment also supported the location of the latter formamide in the upper aromatic cavity of the CC (Fig. S55†). Moreover, the ROESY experiment also displayed intramolecular close-contact cross-peaks between the formyl protons at the two ends of included **8** and their respective α-CH_2 groups, H^1 and H^4 (Fig. 6). This result indicated the selective inclusion of the *cis*,*cis*-isomer of **8** in the cavity of $[\mathbf{2}\cdot Pd]^{6+}$. Bis-formamide **8** exists in solution as a mixture of three isomers with respect to the conformation adopted by the two terminal amides: *trans*,*trans* (∼72%), *trans*,*cis* (∼25%) and *cis*,*cis* (∼3%). The $[\mathbf{2}\cdot Pd]^{6+}$ CC selectively binds the *cis*,*cis*-isomer, most likely in a fully extended conformation (Fig. 5a, right). The binding of long-chain α,ω-bis-

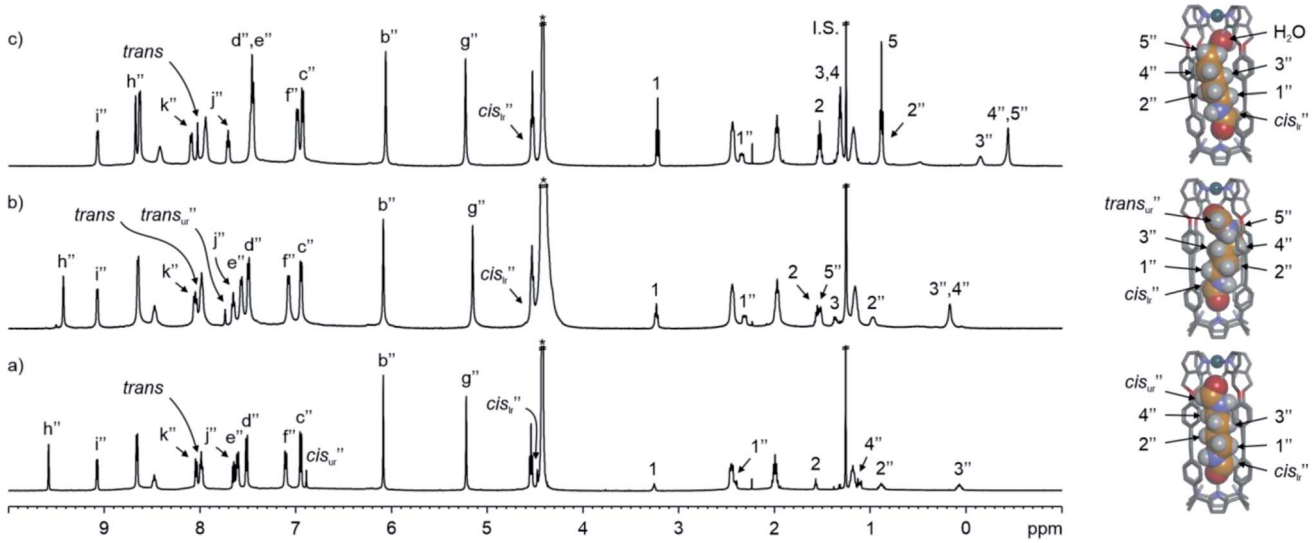

Fig. 5 (Left) ^{1}H NMR (500 MHz with a cryoprobe, D_2O, 333 K) spectra of (a) *cis*,*cis*-**8**⊂[**2**·Pd]$^{6+}$, (b) *trans*,*cis*-**9**⊂[**2**·Pd]$^{6+}$ and (c) *cis*-**10**⊂[**2**·Pd]$^{6+}$, together with free guests in solution. (Right) Energy minimized structures (MM3) of the simplified CC complexes. A putative water molecule is bound to *cis*-**10**⊂[**2**·Pd]$^{6+}$. Double primed labels correspond to the proton signals of the CC complexes (lr = lower rim and ur = upper rim). See Fig. 2a for the proton assignment of bound **2**$^{4+}$. I.S. = *tert*-butanol. *Residual solvent peak.

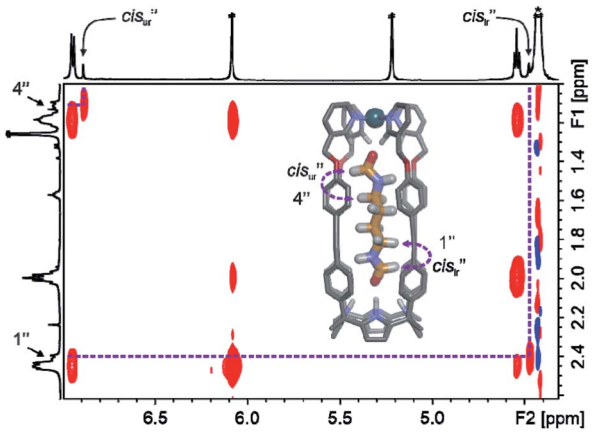

Fig. 6 Selected region of the 2D ROESY NMR (500 MHz with a cryoprobe, D_2O, 333 K, spin lock = 0.3 s) spectrum of *cis*,*cis*-**8**⊂[**2**·Pd]$^{6+}$. Intramolecular close-contacts are indicated in the energy minimized structure (MM3) of the simplified CC complex. Double primed labels correspond to the proton signals of the included guest in the CC.

formamides to a water-soluble resorcin[4]arene deep cavitand was previously investigated by the Rebek group.[49] The cavitand displayed a reduced binding preference for the *trans*,*cis*-isomer compared to the *trans*,*trans*-counterpart. To the best of our knowledge, the high binding selectivity of the [**2**·Pd]$^{6+}$ CC is unprecedented.

We estimated that the stability constant for the *cis*,*cis*-**8**⊂[**2**·Pd]$^{6+}$ CC complex should be larger than 10^5 M^{-1}. The inwardly directed α-pyridyl protons, H^h, in *cis*,*cis*-**8**⊂[**2**·Pd]$^{6+}$ were shifted further downfield than those in the **5**⊂[**2**·Pd]$^{6+}$ complex (9.58 *vs.* 9.09 ppm, respectively).

The homologated bis-formamide **9** (Fig. 2b), possessing an extra methylene group, produced similar results (Fig. 5b). However, the ROESY experiment of the **9**⊂[**2**·Pd]$^{6+}$ CC complex indicated that the CC showed binding selectivity for the *trans*,*cis*-isomer of **9** (Fig. 5b, right) instead of the *cis*,*cis*-counterpart observed in the case of **8**.

The DOSY NMR experiments performed with *cis*,*cis*-**8**⊂[**2**·Pd]$^{6+}$ and *trans*,*cis*-**9**⊂[**2**·Pd]$^{6+}$ yielded similar diffusion constant values (log $D = -9.32$ and -9.31, respectively) to those of the two CC complexes (Fig. S58 and S67†). The calculated magnitudes are almost identical to that determined for the **5**⊂[**2**·Pd]$^{6+}$ counterpart (*vide supra*), supporting the structural size and shape similarity of the three diffusing species.

The binding geometries assigned in water solution to the included bis-formamides in *cis*,*cis*-**8**⊂[**2**·Pd]$^{6+}$ and *trans*,*cis*-**9**⊂[**2**·Pd]$^{6+}$ were in complete agreement with those obtained from X-ray diffraction analyses of single crystals grown for the structural analogues of CC complexes: *cis*,*cis*-**8**⊂[**1a**·Pd]$^{2+}$ and *trans*,*cis*-**9**⊂[**1a**·Pd]$^{2+}$ (Fig. 7a and b). The X-ray structure of *trans*,*cis*-**9**⊂[**1a**·Pd]$^{2+}$ evidenced the bending of the larger alkyl spacer to better adapt to the dimensions of the CC's cavity. The formamide end of **9** hydrogen-bonded to the C[4]P unit adopts the *cis*-conformation, while the opposite end, included in the upper aromatic cavity of the CC, remains in the *trans*-configuration.

The carboxyl oxygen atom of the *trans*-formamide is hydrogen-bonded to the inwardly directed α-pyridyl protons of the CC. The groups of Rebek and Gibb previously reported examples of unusual conformations adopted by alkyl chains of encapsulated guests in self-assembled dimeric capsules.[50–52]

The results with the pyridine *N*-oxide **6** suggested that the assembly of the CC requires the co-inclusion of a water molecule to properly fill the space. We tested the generality of this notion with the monotopic *N*-pentylformamide **10** (Fig. 2b). The ^{1}H NMR spectra of an equimolar mixture of **10** and **2**$^{4+}$ in D_2O solution at 333 K showed the formation of the corresponding **10**⊂**2**$^{4+}$ inclusion complex to a significant extent (Fig. S69†). The addition

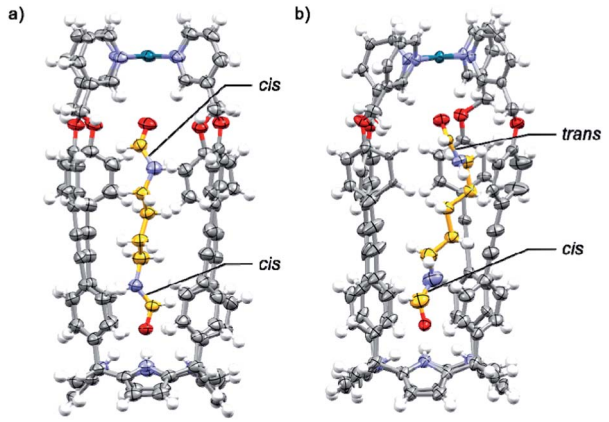

Fig. 7 X-ray crystal structures of (a) *cis,cis*-**8**⊂[**1a**·Pd]$^{2+}$ and (b) *trans,cis*-**9**⊂[**1a**·Pd]$^{2+}$. The structures are shown in ORTEP view with thermal ellipsoids set at 50% probability for the non-hydrogen atoms. Hydrogen atoms are depicted as fixed-size spheres of 0.3 Å radius.

of Pd(II) to this partially formed complex produced a set of sharp signals indicative of the assembly of the **10**⊂[**2**·Pd]$^{6+}$ CC complex (Fig. 5c). Using an internal standard, we determined that the CC complex was assembled to a 60% extent.

The upfield shift experienced by the formyl proton (*cis*″$_{Ir}$, $\Delta\delta$ = −3.46 ppm) of bound **10** placed it in the C[4]P unit. The conformation adopted by the formamide guest was determined by a ROESY experiment as exclusively *cis* (Fig. S72†). The inwardly directed α-pyridyl protons, H^h, in the *cis*-**10** complex were less downfield shifted than those in the **6** counterpart (8.68 *vs.* 9.44 ppm, respectively). The co-inclusion of a water molecule in the putative [**10**·H_2O]⊂[**2**·Pd]$^{6+}$ CC complex satisfies the functional complementarity of the binding site induced by metal coordination[46] (Fig. 5c, right). The binding dynamics of this complex are slow on the chemical shift time scale, but intermediate on the diffusion time scale of a DOSY experiment. A typical DOSY experiment ($t_d \sim 200$ ms) assigned a diffusion constant to bound *cis*-**10** that differed from that of [**2**·Pd]$^{6+}$ (Fig. S76†). Likewise, the diffusion constant of free **10** did not coincide with the value determined for the guest alone in solution (Fig. S78†). The use of a shorter diffusion time ($t_d \sim 10$ ms) showed the expected coincidence of diffusion constants for bound *cis*-**10** and [**2**·Pd]$^{6+}$ (Fig. S77†). This finding indicated that the [*cis*-**10**·H_2O]⊂[**2**·Pd]$^{6+}$ CC complex is kinetically less stable[53] than those involving bis-formamide guests (*vide supra*).

In water, the binding of the guests in the polar aromatic cavity of the [**2**·Pd]$^{6+}$ CC is mainly driven by the hydrophobic effect (HE).[38,43] Additional selectivity and affinity in the recognition process come from hydrogen bonds, and NH–π, π–π and CH–π interactions.[42] The HE's role in the binding of the monoformamide **10** is clear: it is efficiently included in the water-soluble [**2**·Pd]$^{6+}$ CC, but it does not bind to the organic-soluble [**1b**·Pd]$^{2+}$ counterpart (Fig. S30†).

Guest uptake and release in the [2·Pd]$^{6+}$ CC

We briefly investigated the uptake and release mechanism/kinetics[6,54,55] of [**2**·Pd]$^{6+}$ using pair-wise competition experiments (Fig. S80 and S81†). The ^{1}H NMR spectra of equimolar D_2O solutions of $\mathbf{2}^{4+}$, $Pd(NO_3)_2$, and guests **6** (pyridine *N*-oxide) and **8** (butane α,ω-bis-formamide) indicated the assembly of [**6**·H_2O]⊂[**2**·Pd]$^{6+}$ and *cis*,*cis*-**8**⊂[**2**·Pd]$^{6+}$ to 30% and 60% extent, respectively. Sharp signals for the remaining free substrates were observed. Next, we added 1 equiv. of the bis-*N*-oxide **5** to the two solutions and, after 30 s, we reanalysed them using ^{1}H NMR spectroscopy. The encapsulated **6** and **8** were completely replaced by **5**, and the **5**⊂[**2**·Pd]$^{6+}$ CC complex was present to a 60% extent in both solutions. The signals of the protons of the released guests increased in intensity in the bulk solution. The results indicate that the **5**⊂[**2**·Pd]$^{6+}$ CC complex is thermodynamically more stable than those of guests **6** and **8**. In addition, the release of the guests triggered by the uptake of **5** is fast on the human time scale (<30 s). We propose a "French doors" mechanism for the in/out exchange process.[37,56] This mechanism has a low energy barrier (∼20 kcal mol^{-1}) and involves the rotation of the four *meso*-aromatic substituents of the CC. It allows the release of encapsulated **6** or **8**, with the simultaneous uptake of the incoming **5** without the dissociation of any of the pyridyl *N*-Pd(II) bonds of the host.[36]

Conclusions

In summary, we described the efficient self-assembly of endohedrally functionalized [**2**·Pd]$^{6+}$ CC complexes in water by inclusion of mono- and ditopic pyridyl *N*-oxide and aliphatic formamide guests – **5**, **6** and **8–10**, respectively. The precursor $\mathbf{2}^{4+}$ shows a strong aggregation tendency that is somewhat reduced in the 1 : 1 inclusion complexes formed with the polar guests. The complexes of [**2**·Pd]$^{6+}$ feature six positive charges, but are still prone to aggregation in D_2O solutions at r.t. An increase in temperature (333 K) or the addition of DMSO (10%) reduces this aggregation tendency. The ditopic guests (**5**, **8** and **9**) complement the two endohedral polar binding sites of the CC and suitably fill its cavity volume. The monotopic guests (**6** and **10**) are bound to the C[4]P unit of the CC and only partially fill its cavity. Accordingly, we surmise that the latter complexes require the co-inclusion of a water molecule bound to the inwardly directed α-pyridyl protons. We encountered conformational selectivity in the encapsulation of bis-formamides, **8** and **9**, by the [**2**·Pd]$^{6+}$ CC: butane bis-formamide **8** is included as the (otherwise) least abundant *cis*,*cis*-conformer in the CC. Finally, we showed that guests **6** and **8** are displaced by the bis-*N*-oxide **5**, quantitatively and rapidly on the human time scale (<30 s). This finding suggested the existence of a "French doors" mechanism for the guest exchange process. The results are rare examples of guest-induced self-assembly/emergence of CCs having polar aromatic cavities in water solution.[57] The conformational selectivity displayed by the [**2**·Pd]$^{6+}$ CC in the encapsulation of bis-formamide **8** is unprecedented.[58,59]

Data availability

Experimental procedures, characterization data, NMR spectra and X-ray crystal structures are provided in the ESI.†

Author contributions

LE and PB designed the research. QS, LE and JDJ performed the experiments. QS, LE, JDJ and PB analysed the data. LE and PB wrote the paper with input from all authors.

Conflicts of interest

There are no conflicts to declare.

Acknowledgements

We thank Gobierno de España MICIN/AEI/FEDER, UE (projects CTQ2017-84319-P and CEX2019-000925-S), the CERCA Programme/Generalitat de Catalunya, and AGAUR (2017 SGR 1123) for financial support. Q. S. thanks the Chinese Research Council for a predoctoral fellowship (2017-06870013). L. E. thanks MECD for a predoctoral fellowship (FPU14/01016). We also thank Dr Eduardo C. Escudero-Adán for X-ray crystallography data, Dr Gemma Aragay for help with mass spectrometry experiments and Miss Inmaculada Sempere for synthetic assistance.

Notes and references

‖ The tetra-pyridyl SAE-ligand $\mathbf{2}^{4+}$ became soluble in D_2O at mM concentrations after heating the initial suspension at 50–60 °C for 1 h.

** All our attempts to characterize the CC complexes in the gas-phase were unsuccessful. We only detected ion-peaks for the CC in different charged states.

†† The addition of *ca.* 10% DMSO to the r.t. D_2O solution of the $\mathbf{5}\subset[\mathbf{2}\cdot Pd]^{6+}$ CC complex provoked the appearance of sharp proton signals that coincided with those observed at 333 K.

1 M. Fujita, M. Tominaga, A. Hori and B. Therrien, *Acc. Chem. Res.*, 2005, **38**, 369–378.
2 R. Chakrabarty, P. S. Mukherjee and P. J. Stang, *Chem. Rev.*, 2011, **111**, 6810–6918.
3 E. G. Percástegui, T. K. Ronson and J. R. Nitschke, *Chem. Rev.*, 2020, **120**, 13480–13544.
4 M. Fujita, K. Umemoto, M. Yoshizawa, N. Fujita, T. Kusukawa and K. Biradha, *Chem. Commun.*, 2001, 509–518.
5 A. Galan and P. Ballester, *Chem. Soc. Rev.*, 2016, **45**, 1720–1737.
6 T. Y. Kim, R. A. S. Vasdev, D. Preston and J. D. Crowley, *Chem.–Eur. J.*, 2018, **24**, 14878–14890.
7 L. L. K. Taylor, I. A. Riddell and M. M. J. Smulders, *Angew. Chem., Int. Ed.*, 2019, **58**, 1280–1307.
8 M. Morimoto, S. M. Bierschenk, K. T. Xia, R. G. Bergman, K. N. Raymond and F. D. Toste, *Nat. Catal.*, 2020, **3**, 969–984.
9 L. Adriaenssens and P. Ballester, *Chem. Soc. Rev.*, 2013, **42**, 3261–3277.
10 P. M. Bogie, T. F. Miller and R. J. Hooley, *Isr. J. Chem.*, 2019, **59**, 130–139.
11 M. Tominaga, K. Suzuki, T. Murase and M. Fujita, *J. Am. Chem. Soc.*, 2005, **127**, 11950–11951.
12 Q.-Q. Wang, S. Gonell, S. H. A. M. Leenders, M. Dürr, I. Ivanović-Burmazović and J. N. H. Reek, *Nat. Chem.*, 2016, **8**, 225–230.
13 M. D. Johnstone, E. K. Schwarze, J. Ahrens, D. Schwarzer, J. J. Holstein, B. Dittrich, F. M. Pfeffer and G. H. Clever, *Chem.–Eur. J.*, 2016, **22**, 10791–10795.
14 X. Schaapkens, E. O. Bobylev, J. N. H. Reek and T. J. Mooibroek, *Org. Biomol. Chem.*, 2020, **18**, 4734–4738.
15 H. Dasary, R. Jagan and D. K. Chand, *Inorg. Chem.*, 2018, **57**, 12222–12231.
16 X. Schaapkens, J. H. Holdener, J. Tolboom, E. O. Bobylev, J. N. H. Reek and T. J. Mooibroek, *ChemPhysChem*, 2021, **22**, 1187–1192.
17 R. Custelcean, J. Bosano, P. V. Bonnesen, V. Kertesz and B. P. Hay, *Angew. Chem., Int. Ed.*, 2009, **48**, 4025–4029.
18 R. Custelcean, P. V. Bonnesen, N. C. Duncan, X. Zhang, L. A. Watson, G. Van Berkel, W. B. Parson and B. P. Hay, *J. Am. Chem. Soc.*, 2012, **134**, 8525–8534.
19 S. Yi, V. Brega, B. Captain and A. E. Kaifer, *Chem. Commun.*, 2012, **48**, 10295–10297.
20 M. C. Young, L. R. Holloway, A. M. Johnson and R. J. Hooley, *Angew. Chem., Int. Ed.*, 2014, **53**, 9832–9836.
21 L. R. Holloway, P. M. Bogie, Y. Lyon, C. Ngai, T. F. Miller, R. R. Julian and R. J. Hooley, *J. Am. Chem. Soc.*, 2018, **140**, 8078–8081.
22 C. Ngai, C. M. Sanchez-Marsetti, W. H. Harman and R. J. Hooley, *Angew. Chem., Int. Ed.*, 2020, **59**, 23505–23509.
23 D. Zhang, T. K. Ronson, J. Mosquera, A. Martinez, L. Guy and J. R. Nitschke, *J. Am. Chem. Soc.*, 2017, **139**, 6574–6577.
24 D. Zhang, T. K. Ronson, J. Mosquera, A. Martinez and J. R. Nitschke, *Angew. Chem., Int. Ed.*, 2018, **57**, 3717–3721.
25 L. Escobar, D. Villarón, E. C. Escudero-Adán and P. Ballester, *Chem. Commun.*, 2019, **55**, 604–607.
26 Z. Yan, S. Xia, M. Gardlik, W. Seo, V. Maslak, J. Gallucci, C. M. Hadad and J. D. Badjić, *Org. Lett.*, 2007, **9**, 2301–2304.
27 S. Rieth, Z. Yan, S. Xia, M. Gardlik, A. Chow, G. Fraenkel, C. M. Hadad and J. D. Badjić, *J. Org. Chem.*, 2008, **73**, 5100–5109.
28 S. Stojanović, D. A. Turner, C. M. Hadad and J. D. Badjić, *Chem. Sci.*, 2011, **2**, 752–759.
29 F.-U. Rahman, Y.-s. Li, I. D. Petsalakis, G. Theodorakopoulos, J. Rebek and Y. Yu, *Proc. Natl. Acad. Sci. U. S. A.*, 2019, **116**, 17648–17653.
30 M. Petroselli, V. Angamuthu, F.-U. Rahman, X. Zhao, Y. Yu and J. Rebek, *J. Am. Chem. Soc.*, 2020, **142**, 2396–2403.
31 F.-U. Rahman, J.-M. Yang, Y.-H. Wan, H.-B. Zhang, I. D. Petsalakis, G. Theodorakopoulos, J. Rebek and Y. Yu, *Chem. Commun.*, 2020, **56**, 6945–6948.
32 Y.-H. Wan, F.-U. Rahman, J. Rebek Jr and Y. Yu, *Chin. J. Chem.*, 2021, **39**, 1498–1502.
33 H.-B. Zhang, K. Kanagaraj, J. Rebek and Y. Yu, *J. Org. Chem.*, 2021, **86**, 8873–8881.
34 S. Peng, Q. He, G. I. Vargas-Zúñiga, L. Qin, I. Hwang, S. K. Kim, N. J. Heo, C.-H. Lee, R. Dutta and J. L. Sessler, *Chem. Soc. Rev.*, 2020, **49**, 865–907.
35 S. Mecozzi and J. Rebek Jr, *Chem.–Eur. J.*, 1998, **4**, 1016–1022.
36 L. Escobar, E. C. Escudero-Adán and P. Ballester, *Angew. Chem., Int. Ed.*, 2019, **58**, 16105–16109.
37 K. N. Houk, K. Nakamura, C. Sheu and A. E. Keating, *Science*, 1996, **273**, 627–629.

38 L. Escobar and P. Ballester, *Chem. Rev.*, 2021, **121**, 2445–2514.
39 M. A. Beatty and F. Hof, *Chem. Soc. Rev.*, 2021, **50**, 4812–4832.
40 J. Dong and A. P. Davis, *Angew. Chem., Int. Ed.*, 2021, **60**, 8035–8048.
41 L. Escobar and P. Ballester, *Org. Chem. Front.*, 2019, **6**, 1738–1748.
42 E. A. Meyer, R. K. Castellano and F. Diederich, *Angew. Chem., Int. Ed.*, 2003, **42**, 1210–1250.
43 N. E. Ernst and B. C. Gibb, in *Supramolecular Chemistry in Water*, ed. S. Kubik, Wiley-VCH, 2019, pp. 1–33.
44 L. Avram and Y. Cohen, *Chem. Soc. Rev.*, 2015, **44**, 586–602.
45 Y. Cohen, S. Slovak and L. Avram, *Chem. Commun.*, 2021, **57**, 8856–8884.
46 B. Htan, D. Luo, C. Ma, J. Zhang and Q. Gan, *Cryst. Growth Des.*, 2019, **19**, 2862–2868.
47 Q. Sun, L. Escobar and P. Ballester, *Angew. Chem., Int. Ed.*, 2021, **60**, 10359–10365.
48 L. Escobar, A. Díaz-Moscoso and P. Ballester, *Chem. Sci.*, 2018, **9**, 7186–7192.
49 Y.-S. Li, L. Escobar, Y.-J. Zhu, Y. Cohen, P. Ballester, J. Rebek and Y. Yu, *Proc. Natl. Acad. Sci. U. S. A.*, 2019, **116**, 19815–19820.
50 J. J. Rebek, *Chem. Commun.*, 2007, 2777–2789.
51 K.-D. Zhang, D. Ajami and J. Rebek, *J. Am. Chem. Soc.*, 2013, **135**, 18064–18066.
52 S. Liu, D. H. Russell, N. F. Zinnel and B. C. Gibb, *J. Am. Chem. Soc.*, 2013, **135**, 4314–4324.
53 L. Escobar, Y.-S. Li, Y. Cohen, Y. Yu, J. Rebek Jr and P. Ballester, *Chem.–Eur. J.*, 2020, **26**, 8220–8225.
54 M. M. J. Smulders and J. R. Nitschke, *Chem. Sci.*, 2012, **3**, 785–788.
55 S. Akine and Y. Sakata, *Chem. Lett.*, 2020, **49**, 428–441.
56 S. Rieth, K. Hermann, B.-Y. Wang and J. D. Badjić, *Chem. Soc. Rev.*, 2011, **40**, 1609–1622.
57 D. Yang, L. K. S. von Krbek, L. Yu, T. K. Ronson, J. D. Thoburn, J. P. Carpenter, J. L. Greenfield, D. J. Howe, B. Wu and J. R. Nitschke, *Angew. Chem., Int. Ed.*, 2021, **60**, 4485–4490.
58 M. D. Pluth, R. G. Bergman and K. N. Raymond, *J. Org. Chem.*, 2008, **73**, 7132–7136.
59 H. Takezawa, K. Shitozawa and M. Fujita, *Nat. Chem.*, 2020, **12**, 574–578.
60 E. Botana, E. Da Silva, J. Benet-Buchholz, P. Ballester and J. de Mendoza, *Angew. Chem., Int. Ed.*, 2007, **46**, 198–201.
61 E. Botana, M. C. Lubinu, E. Da Silva, P. Espinet and J. de Mendoza, *Chem. Commun.*, 2010, **46**, 4752–4754.